

Lap Joint on St.37 Steel Plate with Friction Welding Clamping Method

Widia Setiawan^{1*}, Nugroho Santoso¹, Wiyadi¹, Muhammad Sulistiyo Aji¹, Rachmat Alamin¹, Achsan Tarmudi²

¹Department of Mechanical Engineering, Vocational College, Gadjah Mada University, Bulaksumur, Yogyakarta, Indonesia.

²Akademi Perindustrian (akprind), Kalisahak, Yogyakarta, Indonesia

*Corresponding author: widia_s@ugm.ac.id

Article history:

Received: 3 January 2023 / Received in revised form: 27 March 2023 / Accepted: 4 May 2023

Available online 8 June 2023

ABSTRACT

Friction stir (FW) welding is a relatively fresh method that was created and has been continually refined and adapted to industrial applications due to its benefits. This approach for solid-state joining entails connecting the components at a temperature below their melting point and then heating them up. Clamp joint applications are widely used using external heating and hitting with high strength, but the clamped joints with the FW method are rarely done. The research studied the characteristic of clamped joints at various plate thicknesses using the FW method. In this study, 30 specimens were used in the form of a St.37 low carbon steel plate with a size of 50 mm x 100 mm and a thickness of 3 mm, 5 mm, and 9 mm, and several holes were made with a diameter of 5 mm. The plate was connected by 2 clamps, and 4 clamps then the FW method was conducted in a milling machine. The results indicate that the plates were connected well. The highest hardness value was 256.4 VHN on the FW of 9 mm plate. The microstructure is dominated by ferrite and a little pearlite phase. The largest shear force is 66.54 kN obtained at 4 clamps with a plate thickness of 9 mm, and the lowest is 13.46 kN, obtained at 2 clamps with a plate thickness of 3 mm.

Copyright © 2023. Journal of Mechanical Engineering Science and Technology.

Keywords: Carbon steel, clamping, friction welding, microhardness, microstructure, shear force

I. Introduction

The latest advancements and fundamental mechanisms of a variety of mechanical (form- and force-closed) and metallurgical joining techniques have been presented and explored. It may be assumed that fundamental information is generally available, particularly in mechanical joining, which is frequently used in industrial applications [1]. The Welding Institute introduced friction welding (FW) as a novel welding technique in 1991 to develop a solid-state joining approach. This approach for solid-state joining involves attaching the components at a temperature below their melting point. To produce welded components with fewer residual stresses, defects, and distortion, issues with porosity, the creation of second phases, embrittlement, and cracking connected to the melting phase of the materials can be discussed. The FW approach has lately been widely applied in a variety of sectors, including aircraft, railroads, and automobiles [2].

FW utilizes atom movement in two directions toward the ductile iron-stainless steel interaction [3]. The addition of carbon atoms to stainless steel and chromium and nickel atoms to ductile iron. Carbon enrichment in stainless steel causes the development of



chromium carbides, which are usually found along the grain boundaries. The addition of iron to Cr and Ni resulted in the formation of the alloy ferrite. During steady-state, the temperature in this area may be described thus that the heat generated by metal friction is [4].

The FW method is the welding joint that occurs in the solid phase, and then the joint process is divided into 4 phases, including: 1. The phase before connection; 2. The first contact phase, light load, and oscillation occur; 3. The axial phase is a full load, and oscillation occurs; 4. Axial compression phase (a process of connection). Inertia FW has been used for more than 30 years for joint problems using mechanical technology machines. Heat is obtained from the rotation of the engine spindle, and the connection occurs due to the process of compressive force in the axial direction [5]. FW is a solid-state joining process that produces coalescence in materials, using the heat generated between surfaces through the combination of a mechanically induced rubbing motion and the applied load [6].

FW has a very strong bond because the fully bonded region is highly dependent on the pin geometry and the rotational speed of the machine [7]. Described in detail as well as difficulties in intermetallic layers, welding processes, and interfacial stresses [8]. According to the fluctuation of axial force, the whole friction taper plug welding (FTPW) process consists of four stages: axial feeding, pressing, welding, and forging. The hole-filling process occurs mostly during the welding phase when burn-off is common. The welding duration, burn-off rate, and torque would be affected by changes in rotation speed and welding force [9].

At the conclusion of the welding joint, several furrow-shaped holes arise in the welding interface, and a smooth line appears in the center welding interface, resulting in a nice welding seam [10]. For example, The ultimate tensile strength measurements in all situations were more than the minimum value of 1000 MPa prescribed by the Aerospace Material Specification for the base material in STA condition [11]. The rotational speed, pressure, and materials all impact the joint's mechanical strength. It might progressively develop as the parameter values improve [12],[13].

The clamped joints using the FW method are rarely done. This research aims to determine the characteristic of clamped joints at various plate thicknesses using the FW method. The thickness of the plate to be joined is 3 mm, 5 mm, and 9 mm, using 2 and 4 methods of FW clamping. Macro photos, temperature measurements, micro photos, microhardness, and tensile strength of the joints will be evaluated.

II. Material and Methods

1. Material

The plates used for this study were low-carbon steel St.37 sheets with a length of 100 mm, a width of 50 mm, and a thickness of 3, 5, and 9 mm. For clamps, welding was used low carbon steel St.37 cylindrical, made in diameter of 4 mm, and a length of 7 mm. The joint was designed with milling CNC at 2000 rpm.

2. Methods

2.1. Preparation

Before the clamping process, the low-carbon steel was cut to 200 mm for each plate and punched with an M6 hole at a distance of 25 cm from the edge for the top and bottom. Meanwhile, the center of the plate was punched at a distance of 25 mm. For the detail, we illustrate it in Figure 1. The top and bottom plates served as reinforcement, while the joining material was in the center. The clamping material was inserted into the hole for the FW process.

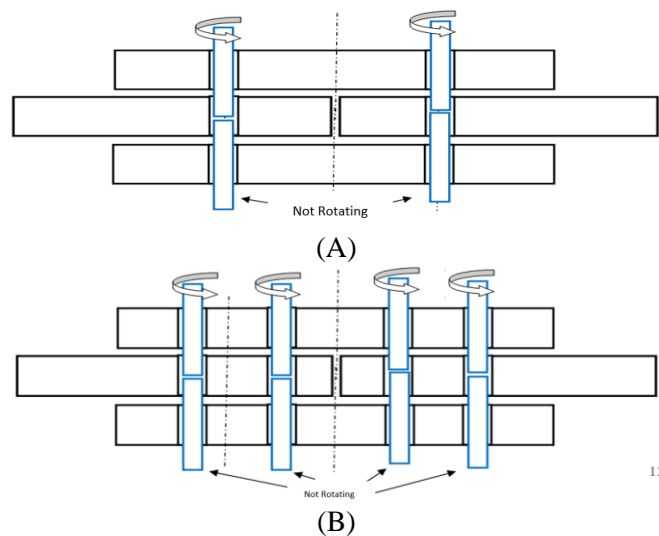


Fig. 1. The process of FW joint: A) Two clamping methods; and B) Four clamping methods.

2.2. Friction Welding Process

The FW process is shown in Figure 2. It used a rotate FW method in a milling machine. The milling machine was switched on, and the top clamp was rotated in counter clock way at 2000 rpm while the bottom clamping was in state condition. The interface rubs against each other, and it took a few seconds to produce heat. Then, the temperature will increase to reach a peak. After reaching the plastic condition, the milling machine was turned off. The upper clamp was pressed on the lower clamp, which was in line with a mechanical bond. This was done for the connection of 2 clamps or 4 clamps. It is expected that the results of the FW process are shown in Figure 3, to consider the appearance and improve the mechanical strength.

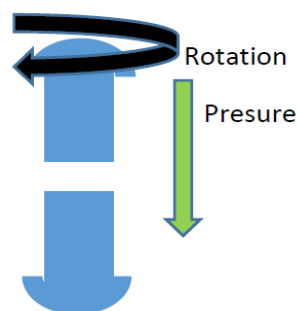


Fig. 2. Clamping used by the FW method.

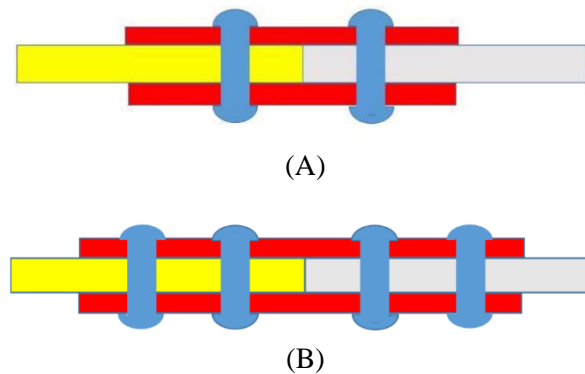


Fig. 3. FW joint design: A) two clamping methods, and B) four clamping methods

2.3. Photo Macro Analysis

The photo macro was used to describe how FW affects the deformation and shape change of the clamp joints. We used heatmap and plotting figures to highlight the areas with defects, especially in the clamp joint area.

2.4. Temperature Analysis

The heat input must be considered to obtain a high connection strength in the process. Heat input was detected using a thermocouple in three positions: top, center, and bottom of the clamp. After the temperature value was obtained, a graph was made to show the temperature changes that occur at each FW time.

2.5. Microstructure Analysis

Microstructure analysis was used to evaluate the phase after the FW method. Microstructure photo observed under a metallurgical microscope with a magnification of 100 times to identify the resulting steel phase and comparison the weld, thermo-mechanically impacted zone (TMAZ), and heat-affected zone (HAZ) area.

2.6. Microhardness Analysis

Vickers microhardness was measured at the clamps along a line. Microhardness was determined by applying a load of 500 g for 10 seconds at a distance of 20 mm among indentations. Six indentations were made on the same surface side of each specimen at various places, with a minimum interval of 1 mm between any two indentations.

2.7. Shear Stress Analysis

Loading was done in the opposite direction of the interface plane. The shear and cross-tension tests were performed in line with ISO 14273. The tests were performed on a universal testing machine weighing 2000 kg and with a set cross-head speed of 10 mm/min. Shear stress in the entire specimen may be calculated by averaging the strengths of three specimens.

III. Results and Discussions

1. Macrostructure

Figure 4 shows the results of the joint with the FW clamping method. It is clear the success of this joint for plate thickness of 3 mm, 5 mm, and 9 mm, also for 2 clamps or 4 clamps. Clamps that are deformed and show open and widened intersections should be avoided to achieve optimum connection strength. On the 3 mm thick plate, deformation occurs in the middle of the clamp. This is due to the meeting of the clamping nail in the top

position and the bottom position, not on the center point. Several factors affect the deformation of the joint, one of which is the thickness of the joint [14]. The thickness affects the material to withstand a force from outside the material. In this study, the 3 mm plate's ability to withstand loads on plates with a thickness of 3 mm is not strong enough and causes deformation.

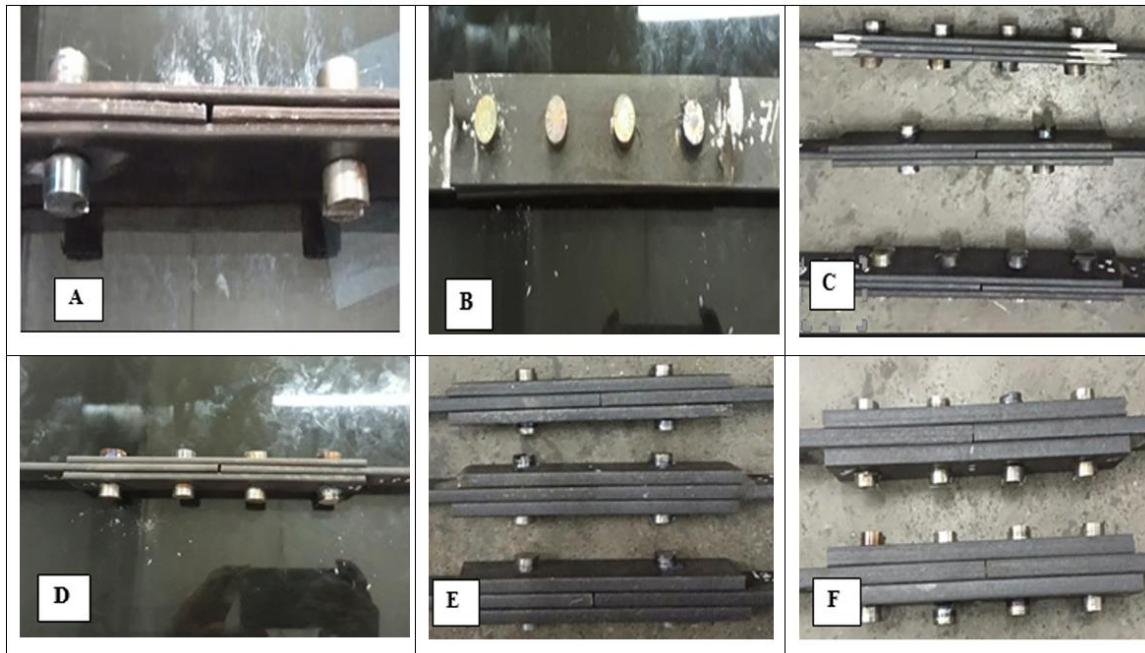


Fig. 4. A) Joint of 2 clamps at 3 mm thick, B) Joint of 4 clamps thick 3 mm, C) Joints 2 clamps plate thickness 5 mm, D) Joints 4 clams plate thickness 5 mm, E) Joint 2 clamps on a plate thickness of 9 mm, F) Joint 4 clamps on a plate thickness of 9 mm.

The misalignment of the clamp nails in the upper and lower positions can also cause deformation because of uneven distribution of the FW twisting force received by the clamp, and ultimately causes deformation [15]. The clamp is also subject to deformation due to welding heating and clamping time [16]. Clamping strongly affects the amplitude of weld distortion, possibly changing the distortion mode and enlarging into deformation [17]. The clamping distance significantly impacts the ultimate distortion; the closer the clamp is to the weld, the less distortion there will be. If the clamp is near the weld seam, the clamp's release time also affects the final distortion; as the release time increases, the distortion decreases [18].

2. Temperature Distribution

Figure 5 shows the temperature distribution at the upper position of the clamp rotates at 2000 rpm, and the lower position of the clamp is stationary. The temperature after a few moments later rises. For the FW clamping process, the temperatures are below 300°C. The maximum temperature during the welding process is 256.7°C with a plate thickness of 3 mm and 5 mm. For 9 mm, the temperature is around 120°C. After the joints melted, the rotation was stopped, clamping was done, and a mechanical joint occurred. The clamp joint was let cooled with air room to make grain growth on clamp joint materials [19] and can be analyzed with a microscope. The heat generated during welding is the combined effect of frictional and physical heating due to the plasticity of the stirred material [20],[21]. The difference in

the thermal rate is quite apparent in thermocouples 1, 2, and 3 are caused by the temperature is not distributed uniformly because of the resistance of the St.37 material [22]. Rotation speed, friction pressure, and welding time are responsible for the speed of heat generation, while the dimensions of the joined materials influence heat generation and also the volume of material generated and stirred during welding [23],[24].

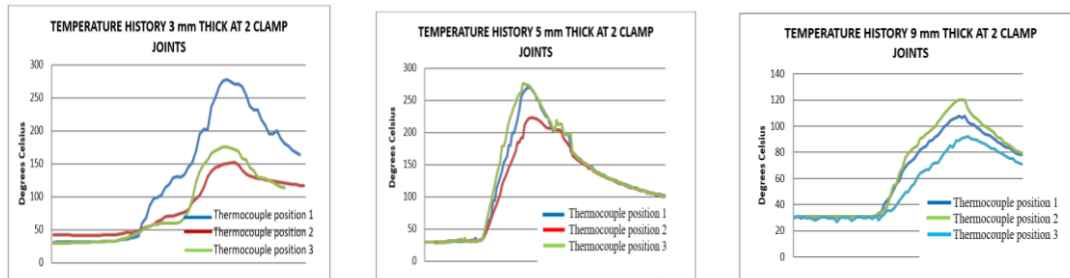


Fig. 5. Temperature distribution for plate thickness of 3 mm, 5 mm, and 9 mm

3. Microstructure

Figure 6 shows the microstructure of 3mm, 5 mm, and 9 mm plates in the weld metal, TMAZ, and HAZ areas with 100x magnification. The ferrite phase has white (light), while pearlite is black (dark), but the grain size of ferrite can also be smaller than pearlite [25]. For detail, the red arrow in Figure 6 shows the pearlite phase formed, while the yellow arrow shows the ferrite phase. Because it does not involve filler material, the microstructure in the weld metal region is ferrite and perlite, with greater ferrite content than perlite. FW merely includes grain refinement of atoms without phase change [26].

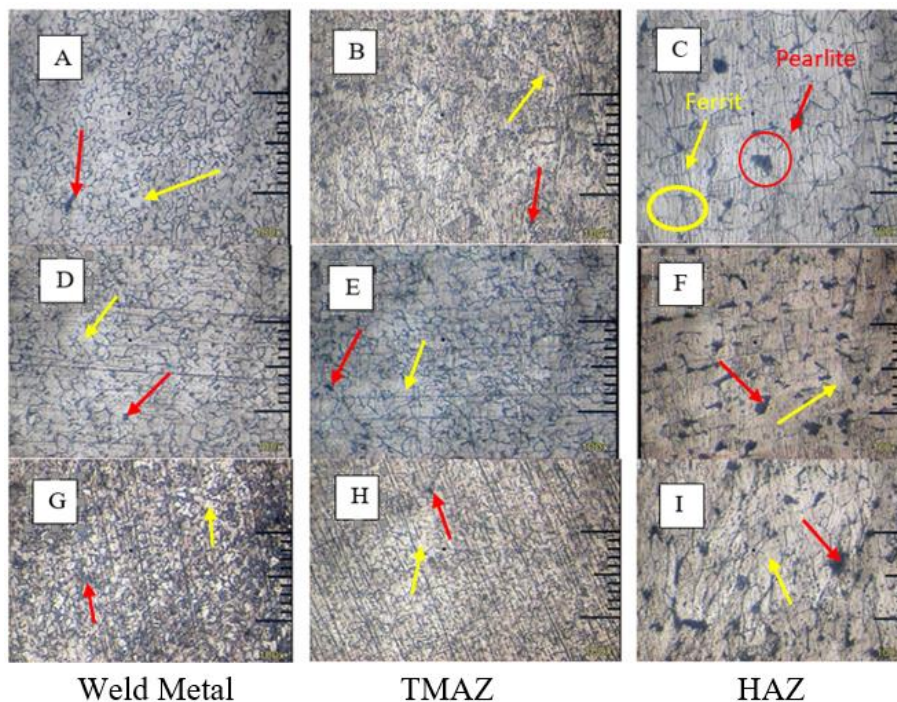


Fig. 6. Microstructure of joint clamps with thickness of 3 mm (A-C), 5 mm (D-F), and 9 mm (G-I)

The side of the stir zone (weld metal) deformation due to the heat of St.37 steel in the austenite region produce small austenite grains, and these grains turn into fine ferrite and pearlite during the cooling process of the material after the welding process [27]. As a result of the higher ferrite content, the material has ductile and soft properties. The fineness of the grains in the weld metal region (weld meta) increases the hardness value and tensile strength of the weld joint [28],[29]. The fine-grained microstructure is generated due to increased rotational speed and frictional pressure [24]. The TMAZ is a transition zone between the stir zone (SZ) and the HAZ with recrystallization similar to the stir zone. In this area, deformed grains have a fine size [30].

The microstructural characterization of the weld region revealed the formation of a fine structure consisting of a mixture of virgin martensite and some stable retained austenite in the CR region, whereas the microstructures of the HAZ and TMAZ revealed the presence of virgin martensite plus δ -ferrite [31]. The microstructure of HAZ is identical to that of the parent metal as it is not subjected to stirring [32]. The difference in heat value is quite obvious in thermocouples 1, 2, and 3 because the temperature is not uniformly distributed due to the resistance of the St.37 material. This difference in heat can affect the length of the HAZ that occurs [22].

4. Microhardness Tests

The microhardness test used micro-Vickers, carried out at 6 stepping points, including the clamping head, each given a distance of 500 μm , to assess the trend of hardness at the joint and to analyze the strength of the joint. From Figure 7, Vickers microhardness increases in friction area 5 of the interface of the specimen with plate 9 mm. The highest value of Vickers microhardness occurs in area 5 in each sample, where the highest values are 191.63 VHN in specimens of 3 mm plates, 167.92 in specimens of 5 mm plates, and 256.4 VHN in specimens of 9 mm plates.

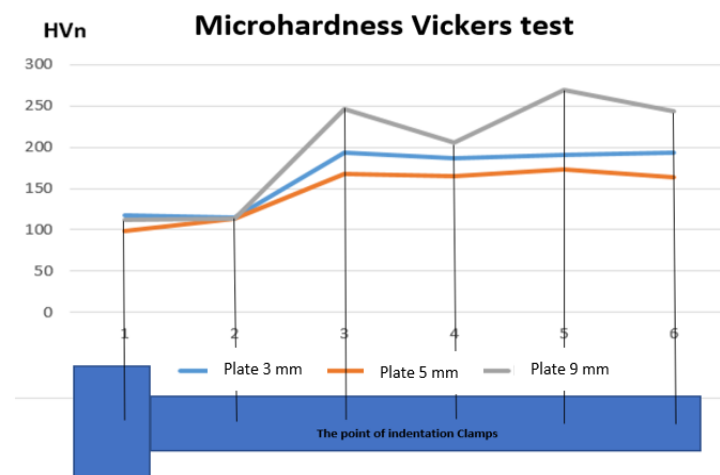


Fig. 7. Vickers microhardness test of plate

The specimen has the highest hardness in area 5 with a temperature of 120°C rotation speed of 2000 rpm. It is caused by a change of microstructure in the interface area with a fine structure of ferrite [33]. A fine microstructure is obtained from increased stress during welding [34]. This result has the same as other research about stainless-steel pipes. Their friction-welded microstructures and local mechanical characteristics (hardness, fracture toughness, and micro-tensile strength) were studied. Formation of a delicate structure composed of virgin martensite and some stable austenite. The existence of virgin martensite

plus d-ferrite, on the other hand, was discovered in the microstructures of HAZ and TMAZ [35].

The changes in the microstructure at various weld locations are closely related to variations in hardness; as the temperature rises, the grain size tends to become smaller and make the material become brittle characteristic [36]. The hardening of the material is affected by rotary friction, axial pressure, and becomes a force with the friction pressure and forging pressure that occurs during welding [37]. These forces cause increased friction and ultimately increase the hardness and Young's modulus of each zone on the steel side [38], but the hardness was decreased caused by high heat energy on the joining interface will have oxide trapped in the nugget and finally reduce the mechanical properties, especially hardness [39].

5. Shear Force Tests

In Figure 8, the plate thickness and the number of clamps affect the resulting shear stress rate because the more clamps and plate thickness used, the resistance of the connection will be greater, and the force required to break will be even larger. The results of FW using 2 clamps with clamp thicknesses of 3, 5, and 9 which were carried out 3 times during the experiment, had an average shear force of 13.46 kN, 28.76 kN, and 32.33 kN, respectively. FW using 4 clamps with 3, 5, and 9 mm clamp thicknesses was carried out 3 times. It results in an average shear force of 50.87 kN, 58.32 kN, and 66.54 kN, respectively.

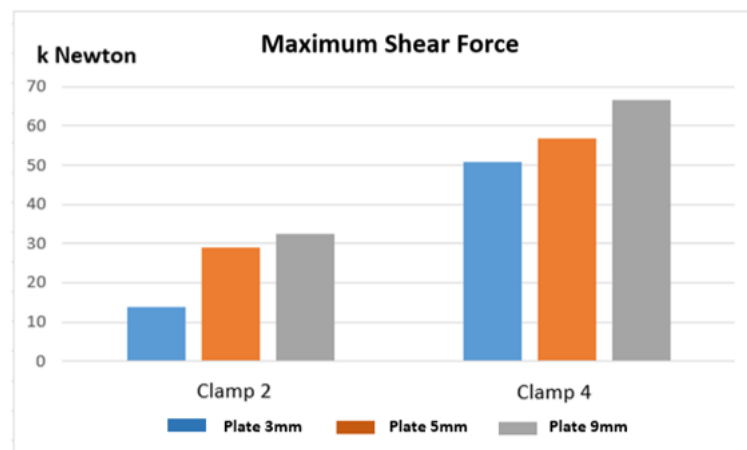


Fig. 8. Maximum shear force of clamp joints

A joint clamp with FW on a plate with a plate thickness of 3 mm has the lowest shear value. This occurs because the clamp with a thickness of 3 mm is deformed during welding so that the load distribution on the plate is uneven, ultimately decreasing its strength [14]. It is possible to extend the welding time and increase the heat input to increase the shear strength of the joint [40]. It will give the melting metals time and opportunity to bond with each other and create an interlocking mechanism that ultimately increases the material's mechanical strength [41].

IV. Conclusions

Based on an analysis of the results of the study, the temperature distribution rapidly increases from the thin plate's thickness of 3 mm to 5 mm. The lowest temperature is 120°C on a 9 mm plate, while the highest is 250.70 °C on a thin plate. The microstructure in the

weld metal and TMAZ areas exhibits grain refinement with ferrite and pearlite phases dominating the friction and heating processes. The highest hardness value was shown in area 5 of each sample with hardness values of 191.63 VHN on 3 mm plate, 167.92 VHN on 5 mm plate, and 256.4 VHN on 9 mm plate. The average tensile test shows that the highest shear force is 4 clamp joints with a maximum shear force of 66.54 kN.

Acknowledgment

This research was funded by Damas Vocational School, Gadjah Mada University. Thank you to the Mechanical Engineering Department for providing laboratory facilities and the Ist Akprind Yogyakarta Laboratory majoring in Mechanical Engineering.

References

- [1] P. Groche, S. Wohletz, M. Brenneis, C. Pabst, and F. Resch, "Joining by forming - A review on joint mechanisms, applications and future trends," *J. Mater. Process. Technol.*, vol. 214, no. 10, pp. 1972–1994, 2014, doi: 10.1016/j.jmatprotec.2013.12.022.
- [2] M. Soori, M. Asmael, and D. Solyall, "Recent Development in Friction Stir Welding Process: A Review," *SAE Int. J. Mater. Manuf.*, vol. 14, no. 1, pp. 63–80, 2020, doi: 10.4271/05-14-01-0006.
- [3] Z. Jiao, C. Song, T. Lin, and P. He, "Molecular dynamics simulation of the effect of surface roughness and pore on linear friction welding between Ni and Al," *Comput. Mater. Sci.*, vol. 50, no. 12, pp. 3385–3389, 2011, doi: 10.1016/j.commatsci.2011.06.033.
- [4] J. T. Xiong, J. L. Li, Y. N. Wei, F. S. Zhang, and W. D. Huang, "An analytical model of steady-state continuous drive friction welding," *Acta Mater.*, vol. 61, no. 5, pp. 1662–1675, 2013, doi: 10.1016/j.actamat.2012.11.042.
- [5] K. S. Mortensen, C. G. Jensen, L. C. Conrad, and F. Losee, "Mechanical properties and microstructures of inertia-friction-welded 416 stainless steel," *Weld. J. (Miami, Fla)*, vol. 80, no. 11, 2001.
- [6] R. Winiczenko and M. Kaczorowski, "Friction welding of ductile iron with stainless steel," *J. Mater. Process. Technol.*, vol. 213, no. 3, pp. 453–462, 2013, doi: 10.1016/j.jmatprotec.2012.10.008.
- [7] Tiwan, M. N. Iلمان, and Kusmono, "Microstructure and mechanical properties of friction stir spot welded AA5052-H112 aluminum alloy," *Heliyon*, vol. 7, no. 2, p. e06009, 2021, doi: 10.1016/j.heliyon.2021.e06009.
- [8] P. Rombaut, W. De Waele, and K. Faes, "Friction welding of steel to ceramic," *Int. J. Sustain. Constr. Des.*, vol. 2, no. 3, pp. 448–457, 2011, doi: 10.21825/scad.v2i3.20544.
- [9] L. Cui, X. Yang, D. Wang, J. Cao, and W. Xu, "Experimental study of friction taper plug welding for low alloy structure steel: Welding process, defects, microstructures and mechanical properties," *Mater. Des.*, vol. 62, pp. 271–281, 2014, doi: 10.1016/j.matdes.2014.05.026.
- [10] J. Luo, J. Xiang, D. Liu, F. Li, and K. Xue, "Radial friction welding interface between brass and high carbon steel," *J. Mater. Process. Technol.*, vol. 212, no. 2, pp. 385–

- 392, 2012, doi: 10.1016/j.jmatprotec.2011.10.001.
- [11] R. Damodaram, S. Ganesh Sundara Raman, D. V. V. Satyanarayana, G. Madhusudhan Reddy, and K. Prasad Rao, "Hot tensile and stress rupture behavior of friction welded alloy 718 in different pre-and post-weld heat treatment conditions," *Mater. Sci. Eng. A*, vol. 612, pp. 414–422, 2014, doi: 10.1016/j.msea.2014.06.076.
- [12] N. S. Kalsi and V. S. Sharma, "A statistical analysis of rotary friction welding of steel with varying carbon in workpieces," *Int. J. Adv. Manuf. Technol.*, vol. 57, no. 9–12, pp. 957–967, 2011, doi: 10.1007/s00170-011-3361-z.
- [13] F. Jin, J. Li, P. Liu, X. Nan, X. Li, J. Xiong, and F. Zhang, "Friction coefficient model and joint formation in rotary friction welding," *J. Manuf. Process.*, vol. 46, no. September, pp. 286–297, 2019, doi: 10.1016/j.jmapro.2019.09.008.
- [14] T. Schenk, M. Doig, G. Esser, and I. M. Richardson, "Influence of clamping support distance on distortion of welded T joints," *Sci. Technol. Weld. Join.*, vol. 15, no. 7, pp. 575–582, Oct. 2010, doi: 10.1179/136217110X12731414739835.
- [15] W. Liang and D. Deng, "Influences of heat input, welding sequence and external restraint on twisting distortion in an asymmetrical curved stiffened panel," *Adv. Eng. Softw.*, vol. 115, pp. 439–451, Jan. 2018, doi: 10.1016/j.advengsoft.2017.11.002.
- [16] T. Schenk, I. M. Richardson, M. Kraska, and S. Ohnimus, "A study on the influence of clamping on welding distortion," *Comput. Mater. Sci.*, vol. 45, no. 4, pp. 999–1005, Jun. 2009, doi: 10.1016/j.commatsci.2009.01.004.
- [17] M. Seyyedean Choobi, M. Haghpanahi, and M. Sedighi, "Investigation of the effect of clamping on residual stresses and distortions in butt-welded plates," *Sci. Iran.*, vol. 17, no. 5 B, pp. 387–394, 2010.
- [18] A. Schober, "Eine Methode zur Wärmequellenkalibrierung in der Schweißstruktursimulation." 2014.
- [19] U. Das and V. Toppo, "Effect of Tool Rotational Speed on Temperature and Impact Strength of Friction Stir Welded Joint of Two Dissimilar Aluminum Alloys," *Mater. Today Proc.*, vol. 5, no. 2, pp. 6170–6175, 2018, doi: 10.1016/j.matpr.2017.12.223.
- [20] S. Choudhury, T. Medhi, D. Sethi, S. Kumar, B. S. Roy, and S. C. Saha, "Temperature distribution and residual stress in Friction Stir Welding process," *Mater. Today Proc.*, vol. 26, pp. 2296–2301, 2020, doi: 10.1016/j.matpr.2020.02.496.
- [21] B. Meyghani, M. Awang, C. S. Wu, and S. Emamian, "Temperature Distribution Investigation During Friction Stir Welding (FSW) Using Smoothed-Particle Hydrodynamics (SPH)," 2020, pp. 749–761. doi: 10.1007/978-981-15-5753-8_70.
- [22] N. Shete and S. U. Deokar, "A Review Paper on Rotary Friction Welding," *Int. Conf. Ideas*, vol. 5, no. 6, pp. 1557–1560, 2017.
- [23] S. Absar, B. J. Ruskiewicz, J. D. Skovron, L. Mears, T. Abke, X. Zhao, and H. Choi, "Temperature measurement in friction element welding process with micro thin film thermocouples," *Procedia Manuf.*, vol. 26, pp. 485–494, 2018, doi: 10.1016/j.promfg.2018.07.057.
- [24] M. C. Zulu and P. M. Mashinini, "The influence of rotational speed and pressure on the properties of rotary friction welded titanium alloy (Ti-6Al-4V)," *11th South African Conf. Comput. Appl. Mech. SACAM 2018*, pp. 103–111, 2018.

- [25] G. İpekoğlu, T. Küçükömero, S. M. Aktarer, D. M. Sekban, and G. Çam, "Investigation of microstructure and mechanical properties of friction stir welded dissimilar St37/St52 joints," *Mater. Res. Express*, vol. 6, no. 4, p. 046537, Jan. 2019, doi: 10.1088/2053-1591/aafb9f.
- [26] D. Puspitasari, P. Puspitasari, M. R. G. Firmansyah, and S. Solichin, "The Effect of Rotational Speed, Friction Duration, and Pressure on Tensile Strength of AISI 6061 Welding Joints," *J. Mech. Eng. Sci. Technol.*, vol. 2, no. 1, pp. 38–42, 2018, doi: 10.17977/um016v2i12018p038.
- [27] M. Jafarzaghan, A. H. Feng, A. Abdollah-zadeh, T. Saeid, J. Shen, and H. Assadi, "Microstructural characterization in dissimilar friction stir welding between 304 stainless steel and st37 steel," *Mater. Charact.*, vol. 74, pp. 28–41, Dec. 2012, doi: 10.1016/j.matchar.2012.09.004.
- [28] M. Jafarzaghan, A. Abdollah-zadeh, A. H. Feng, T. Saeid, J. Shen, and H. Assadi, "Microstructure and Mechanical Properties of a Dissimilar Friction Stir Weld between Austenitic Stainless Steel and Low Carbon Steel," *J. Mater. Sci. Technol.*, vol. 29, no. 4, pp. 367–372, Apr. 2013, doi: 10.1016/j.jmst.2013.02.008.
- [29] Y. yohanes and M. Meipen, "Effect of Rotational Speed on Hardness Value and Area of Vertical Bar-Plate Rotary Friction Weld Joint," *J. Ocean. Mech. Aerosp. -science Eng.*, vol. 66, no. 3, pp. 77–81, Nov. 2022, doi: 10.36842/jomase.v66i3.327.
- [30] P. Zolghadr, M. Akbari, and P. Asadi, "Formation of thermo-mechanically affected zone in friction stir welding," *Mater. Res. Express*, vol. 6, no. 8, p. 086558, May 2019, doi: 10.1088/2053-1591/ab1d25.
- [31] C. A. Della Rovere, C. R. Ribeiro, R. Silva, N. G. Alcântara, and S. E. Kuri, "Local mechanical properties of radial friction welded supermartensitic stainless steel pipes," *Mater. Des.*, vol. 56, pp. 423–427, 2014, doi: 10.1016/j.matdes.2013.11.020.
- [32] R. Palanivel, R. F. Laubscher, I. Dinaharan, and D. G. Hattingh, "Microstructure and mechanical characterization of continuous drive friction welded grade 2 seamless titanium tubes at different rotational speeds," *Int. J. Press. Vessel. Pip.*, vol. 154, pp. 17–28, Jul. 2017, doi: 10.1016/j.ijpvp.2017.06.005.
- [33] J.-W. Choi, W. Li, K. Ushioda, M. Yamamoto, and H. Fujii, "Microstructure evolution and hardness distribution of linear friction welded AA5052-H34 joint and AA5083-O joint," *J. Mater. Res. Technol.*, vol. 17, pp. 2419–2430, Mar. 2022, doi: 10.1016/j.jmrt.2022.02.003.
- [34] Y. Lu, X. Zhang, H. Wang, C. Kan, F. Zhang, P. Dai, and H. Wang, "Investigation of microstructure, texture, and mechanical properties of FeCoNiCrMn high entropy alloy during drive friction welding," *Mater. Charact.*, vol. 189, p. 111959, Jul. 2022, doi: 10.1016/j.matchar.2022.111959.
- [35] C. A. Della Rovere, C. R. Ribeiro, R. Silva, L. F. S. Baroni, N. G. Alcântara, and S. E. Kuri, "Microstructural and mechanical characterization of radial friction welded supermartensitic stainless steel joints," *Mater. Sci. Eng. A*, vol. 586, pp. 86–92, 2013, doi: 10.1016/j.msea.2013.08.014.
- [36] M. N. Ilman, A. Widodo, and N. A. Triwibowo, "Metallurgical, Mechanical and Corrosion Characteristics of Vibration Assisted Gas Metal Arc Aa6061-T6 Welded Joints," *SSRN Electron. J.*, 2022, doi: 10.2139/ssrn.4122101.

- [37] H. T. M. Nu, N. H. Loc, and L. P. Minh, "Influence of the rotary friction welding parameters on the microhardness and joint strength of Ti6Al4V alloys," *Proc. Inst. Mech. Eng. Part B J. Eng. Manuf.*, vol. 235, no. 5, pp. 795–805, Apr. 2021, doi: 10.1177/0954405420972549.
- [38] B. Cheniti, D. Miroud, R. Badji, P. Hvizdoš, M. Fides, T. Csanádi, B. Belkessa, and M. Tata, "Microstructure and mechanical behavior of dissimilar AISI 304L/WC-Co cermet rotary friction welds," *Mater. Sci. Eng. A*, vol. 758, pp. 36–46, Jun. 2019, doi: 10.1016/j.msea.2019.04.081.
- [39] W. Setiawan, N. Santoso, and S. Surojo, "New Design of Aluminum 6061 Welding Joining Using Friction Stir Welding Method," *J. Mech. Eng. Sci. Technol.*, vol. 4, no. 2, pp. 135–143, 2020, doi: 10.17977/um016v4i22020p135.
- [40] L. Chen, Y. Zhang, X. Xue, B. Wang, J. Yang, Z. Zhang, N. Tyrer, and G. C. Barber, "Investigation on shearing strength of resistance spot-welded joints of dissimilar steel plates with varying welding current and time," *J. Mater. Res. Technol.*, vol. 16, pp. 1021–1028, Jan. 2022, doi: 10.1016/j.jmrt.2021.12.079.
- [41] Z. Wu, G. Zhang, B. Wang, and K. Shih, "Experimental Investigation on Solid State Resistance Spot Welding," in *Volume 2: Advanced Manufacturing*, American Society of Mechanical Engineers, Nov. 2017. doi: 10.1115/IMECE2017-72581.